

# Line-blanketed model atmospheres for R Coronae Borealis stars and hydrogen-deficient carbon stars

Martin Asplund<sup>1</sup>, Bengt Gustafsson<sup>1</sup>, Dan Kiselman<sup>2,3</sup>, and Kjell Eriksson<sup>1</sup>

<sup>1</sup> Astronomiska observatoriet, Box 515, S-751 20 Uppsala, Sweden

<sup>2</sup> NORDITA, Blegdamsvej 17, DK-2100 Copenhagen Ø, Denmark

<sup>3</sup> present address: Stockholms observatorium, S-133 36 Saltsjöbaden, Sweden

e-mail: martin@astro.uu.se; bg@astro.uu.se; dan@astro.su.se; ke@astro.uu.se

Received 1 May 1996 / Accepted 2 July 1996

**Abstract.** We have constructed line-blanketed model atmospheres for the hydrogen-deficient and carbon-rich R Coronae Borealis (R CrB) stars, as well as for the similar hydrogen-deficient carbon (HdC) stars and the cool extreme helium (EHe) stars. Improved continuum opacities have been used together with realistic line absorption data for atomic and molecular transitions. The observed dereddened fluxes of R CrB are compared with the calculated model fluxes and found to agree best with a model effective temperature of 6 900 K, while the infrared flux method gives between 6 600 and 6 900 K, depending on the nature of the flux excess in the J and H bands compared to the model fluxes. The excess may correspond to a recently formed dust cloud close to the star, with a typical temperature around 2 000 K and a dust mass of  $\sim 10^{-11} M_{\odot}$ . The agreement for the ultraviolet flux distribution is also very satisfactory as seen from *IUE* spectra of R CrB. Theoretical broad band photometry is presented and effective temperatures of R CrB and HdC stars estimated.

The constructed models show a significantly steeper temperature gradient compared to previously existing models as a result of the line opacity. Due to the cool surface and high abundance of carbon, molecular bands of e.g. C<sub>2</sub> and CO are visible in the spectra even at as high effective temperatures as 7 000 K. Furthermore, the high temperatures encountered at depth explain the observed He I and C II lines for  $T_{\text{eff}}$  down to  $\sim 7 000$  K. In the inner layers ( $\tau_{\text{Ross}} \gtrsim 3$ ) the models show density inversions related to the ionization zone of helium. For certain low gravity models the luminosity exceeds the local Eddington limit and hence gas pressure inversions occur as well, which could be related to the decline events of R CrB stars.

**Key words:** stars: model atmospheres – stars: AGB and post-AGB – stars: variables: R Coronae Borealis – stars: variables: luminous blue variables – radiative transfer – instabilities

## 1. Introduction

The variable stars named after the prototype R Coronae Borealis (R CrB stars) continue to puzzle astronomers with unpredictable lightcurves and peculiar chemical compositions. The decline events occur seemingly at random, when the stars fade up to eight magnitudes on a relatively short timescale of weeks, while the recovery to normal light takes months, to a state where it may often remain for several years. It is commonly believed that dense dust formation obscures the star along the line of sight (Loreta 1934), but the trigger mechanism for this dust formation episode is still unknown. Characteristic of the class is also the hydrogen-poor and carbon-rich composition, but with a rather large star to star scatter for certain elements. Therefore the stars may be grouped into distinct subgroups (Lambert & Rao 1994), probably with different evolutionary backgrounds. It has been suggested that the R CrB stars originate in either the merging of two white dwarfs (Webbink 1984) or a final He-shell flash in a cooling white dwarf (Renzini 1979). Possible progenitors and descendants of R CrB stars are found in the Hertzsprung-Russell diagram as hydrogen-deficient carbon stars (HdC) and extreme helium stars (EHe). R CrB stars are thought to be evolving towards higher temperatures as indicated by the change in the pulsation period of RY Sgr (Kilkenny 1982), though this finding is not undisputed (Lombard & Koen 1993).

The effective temperatures of these supergiants range from about 5 000 K for the coolest members to about 20 000 K for the three hot R CrB stars, but with a majority around  $T_{\text{eff}} = 7 000$  K. Unfortunately, determinations of temperatures, gravities and compositions have only been possible for a very limited number of R CrB stars. In order to improve this both high-resolution observations of a larger sample of these stars and better model atmospheres are necessary. Here we address the latter goal by including the effects of line-blanketing. A detailed abundance analysis will be the topic of a subsequent paper (Lambert et al., in preparation). Realistic models of the outer structure of these stars are also important for analysing the possibility of an instability close to or in the stellar atmosphere, causing

events that may trigger the dust condensations and the famous declines. Polarization observations, geometrical considerations and timescales of the declines indicate that the dust must be formed close to the photosphere (Whitney et al. 1992) in spite of the high effective temperatures.

The HdC stars have attracted relatively little attention. The five objects known are similar to the R CrB stars in their chemical composition and the semiregular light curve variations, though lacking the characteristic decline events of the R CrB stars and an infrared excess. One R CrB star, XX Cam, is sometimes also referred to as belonging to the HdC class due to its rare declines and weak IR excess. The only published abundance analysis of HdC stars is due to Warner (1967) and was based on very primitive model atmospheres by modern standards. The effective temperatures are believed to be between 5 000 and 7 000 K.

Model atmospheres for R CrB and related stars have previously been constructed by Schönberner (1975) but without line-blanketing and with now outdated continuum opacities, and Jones (1991) with a modified MARCS code (Gustafsson et al. 1975), utilizing opacity distribution functions (ODF) to approximate the effect of line blanketing but still using old continuum opacities.

In Sect. 2 we present the numerical details and the opacities used for the model atmospheres, while in Sect. 3 we discuss the properties of the models, and in particular their connection with the Eddington limit. Comparisons with previous hydrogen-deficient model atmospheres and the calculated flux distribution with the observed values of R CrB itself are found in Sect. 4 and Sect. 5, respectively. The calculated photometric colours are presented in Sect. 6 and synthetic spectra of relevant line features are shown in Sect. 7.

## 2. Physical input and the numerical details

### 2.1. Assumptions and limitations

The models are based on several necessary assumptions and limitations. The usual approximations of a flux-constant, plane-parallel, hydrostatic atmosphere in local thermodynamic equilibrium (LTE) are made, which no doubt is at best only a crude description of the outer layers of these pulsating supergiants. Nevertheless, this is a useful approach in the absence of more complex and advanced model atmosphere simulations relaxing one or more of the above assumptions. We have investigated the relevance of the plane-parallel and LTE approximations, see below in Sect. 3.6 and Sect. 3.7.

The R CrB stars are hydrogen-poor but overabundant in carbon and nitrogen; helium is, however, still the most abundant element. Unless the C/He ratio is very small or hydrogen is more common than normal, the opacity is mainly determined by carbon through its bound-free and free-free absorption, at least in the line forming regions. Furthermore, carbon is the most important electron donor and hence indirectly affects the contribution from two other important continuum opacity sources: He<sup>-</sup> and electron scattering. This makes the C/He ratio difficult

**Table 1.** Standard chemical composition

Element	log $\epsilon^a$	Element	log $\epsilon^a$
H	7.50	K	4.80
He	11.52	Ca	5.90
C	9.52	Sc	2.80
N	9.40	Ti	4.70
O	8.80	V	3.70
Ne	8.50	Cr	5.40
Na	6.80	Mn	5.10
Mg	7.20	Fe	7.20
Al	6.60	Co	4.60
Si	7.70	Ni	6.50
S	7.50		

<sup>a</sup> Normalized such that  $\log \sum_i \mu_i \epsilon_i = 12.15$ , with  $\mu_i$  denoting the atomic weight of the element

to determine since the equivalent width of a C I line is almost independent of the adopted ratio of these two elements. The equivalent width is also insensitive to the effective temperature and gravity. Helium lines are sometimes present but may suffer from a chromospheric contribution and are also sensitive to the adopted  $T_{\text{eff}}$ . Hence they are not reliable abundance diagnostics.

An idea of the appropriate C/He ratio can, however, be obtained from comparison with the suggested relatives of R CrB stars: EHe stars and the few “hot” R CrB stars where the ratio is determined from C II, C III and He I. The EHe stars have a low ratio, close to 1% (by number) and with a relatively small scatter (Heber 1986) while the three known hot R CrB stars have ratios both significantly higher (V348 Sgr, Leuenhagen & Hamann 1994) and lower (MV Sgr, Jeffery et al. 1988). The third hot R CrB star (DY Cen, Jeffery & Heber 1993) has C/He similar to those of the EHe stars analysed so far. If an evolutionary link between these classes exists, a similar ratio is to be expected for the R CrB stars, and we therefore adopt 1% for the standard grid. We have, however, experimented with a ratio between 0.1% and 10%, as well as varying individual abundances. The abundances used for the standard grid are mainly taken from Lambert & Rao (1994) and, following these authors, normalized to  $\log \sum_i \mu_i \epsilon_i = 12.15$ , with  $\mu_i$  being the atomic weight of the element, and  $\epsilon_i$  the abundance by number, see Table 1.

In the present study we have calculated model atmospheres with parameters in the range  $5\,000 \leq T_{\text{eff}} \leq 9\,500$  K and  $-0.5 \leq \log g \leq 2.0$  [cgs]. Certain low temperature – high gravity and high temperature – low gravity models have not been computed (in the first case since no R CrB or HdC stars are expected to have those parameters; in the second case due to convergence problem caused by too large super-Eddington luminosities, see below in Sect. 3.2). We have adopted a microturbulence of  $\xi_{\text{turb}} = 5$  km s<sup>-1</sup>, mainly because the line opacities for the code are only tabulated for certain choices of  $\xi_{\text{turb}}$  and no interpolation is used, while the observed microturbulence values are typically 5–10 km s<sup>-1</sup> (Lambert et al., in preparation). The effect of the uncertainty in  $\xi_{\text{turb}}$  is discussed in Sect. 3.3.

**Table 2.** Grid parameters

$T_{\text{eff}}$ [K]	$\log g$ [cgs]	Abundance variations
5 000	-0.50	C/He=0.3, 1.0, 3.0%
	0.00	C/He=0.3, 1.0, 3.0%
	0.50	C/He=0.3, 1.0, 3.0%
	1.00	C/He=0.3, 1.0, 3.0%
5 500	-0.50	C/He=0.3, 1.0, 3.0%
	0.00	C/He=0.3, 1.0, 3.0%
	0.50	C/He=0.3, 1.0, 3.0%
	1.00	C/He=0.3, 1.0, 3.0%
6 000	-0.50	C/He=0.3, 1.0, 3.0%
	0.00	C/He=0.1, 0.3, 1.0, 3.0, 10%
	0.50	C/He=0.1, 0.3, 1.0, 3.0, 10%
	1.00	C/He=0.1, 0.3, 1.0, 3.0, 10%
6 500	-0.50	C/He=0.3, 1.0, 3.0%
	0.00	C/He=0.1, 0.3, 1.0, 3.0, 10%
	0.50	C/He=0.1, 0.3, 1.0, 3.0, 10%
	1.00	C/He=0.1, 0.3, 1.0, 3.0, 10%
	1.50	C/He=0.3, 1.0, 3.0%
6 750	0.00	C/He=1.0%
	0.50	C/He=1.0%
	1.00	C/He=1.0%
	1.50	C/He=1.0%
7 000	0.00	C/He=0.1, 0.3, 1.0, 3.0, 10%
	0.50	C/He=0.1, 0.3, 1.0, 3.0, 10%
	1.00	C/He=0.1, 0.3, 1.0, 3.0, 10%
	1.50	C/He=0.3, 1.0, 3.0%
7 250	0.00	C/He=1.0%
	0.50	C/He=1.0%
	1.00	C/He=1.0%
	1.50	C/He=1.0%
	2.00	C/He=0.3, 1.0, 3.0%
7 500	0.00	C/He=0.1, 0.3, 1.0, 3.0, 10%
	0.50	C/He=0.1, 0.3, 1.0, 3.0, 10%
	1.00	C/He=0.1, 0.3, 1.0, 3.0, 10%
	1.50	C/He=0.3, 1.0, 3.0%
8 000	0.50	C/He=0.3, 1.0, 3.0%
	1.00	C/He=0.3, 1.0, 3.0%
	1.50	C/He=0.3, 1.0, 3.0%
	2.00	C/He=0.3, 1.0, 3.0%
	2.50	C/He=0.3, 1.0, 3.0%
8 500	1.00	C/He=0.3, 1.0, 3.0%
	1.50	C/He=0.3, 1.0, 3.0%
	2.00	C/He=0.3, 1.0, 3.0%
9 000	1.00	C/He=0.3, 1.0, 3.0%
	1.50	C/He=0.3, 1.0, 3.0%
	2.00	C/He=0.3, 1.0, 3.0%
9 500	1.00	C/He=0.3, 1.0, 3.0%
	1.50	C/He=0.3, 1.0, 3.0%
	2.00	C/He=0.3, 1.0, 3.0%

A summary of the calculated models is presented in Table 2. A shorter preliminary description of the models was given by Gustafsson & Asplund 1996.

The numerical code solves the radiative transfer problem simultaneously with the equations of hydrostatic equilibrium and flux constancy for the optical depth range  $-4.2 \leq \log \tau_{\text{Ross}} \leq$

1.6) for about 5 500 wavelengths. The method is a combination of the opacity sampling (OS) and the opacity distribution function (ODF) methods, with the latter only used redward of 450 nm. The program is an extension of the original MARCS-code (Gustafsson et al. 1975). Convection is treated through the mixing length theory with the mixing length parameter  $l/H_P = 1.6$ . A very similar version of the code has previously been used in the investigation of the chemical evolution of the Galactic disk by Edvardsson et al. (1993) and found to be stable and quick to converge.

## 2.2. Opacities

### 2.2.1. Continuous opacities

The very different chemical composition of the R CrB stars relative to that of the Sun means that care must be taken when choosing the continuous opacities for the atmospheric models. We have included bound-free absorption for H, He, C, N, O, Mg, Al, Si, Ca and Fe, both for neutral and singly ionised species. For all these, except H and Fe, we have used data from the Opacity Project (Seaton et al. 1994 and references therein) and retrieved from the on-line database TOPbase (Cunto et al. 1993). The photoionization cross-section data in TOPbase is given for each atomic energy term (tens or hundreds of levels per species) with a very fine frequency resolution (several hundred frequency points per level). In many cases the cross-sections show very detailed structure with strong resonances.

In order to reduce the cross-section data for each species the first step was to smooth the cross-sections for each atomic level. This was mainly done in order to ease computer memory requirements. The data for all levels of a species were then multiplied with the appropriate Boltzmann factors (one for each temperature) and added. The resulting curve was inspected and the final wavelength points were chosen for each species so that the remaining resonance structure and the ionization edges in the most important wavelength intervals were reasonably represented.

One may, however, suspect that the initial smoothing will destroy essential properties of the b-f opacity: strong resonance peaks with low absorption in between. Therefore, the procedure was repeated without the presmoothing for Ca I (the species which shows most severe resonance structure in the visual and near ultraviolet parts of the spectrum) and C I (which is the most important of the atomic b-f opacity sources). The impact on the atmospheric structure of these changes was, however, negligible. The resulting b-f absorption coefficients for 26 different temperatures extending from 3000 to 36 000 K are tabulated in the input files for the model atmosphere code.

The free-free opacity of the negative ions of helium (John 1994), carbon (Bell et al. 1988), nitrogen (Ramsbottom et al. 1992) and oxygen (John 1975) are of significance in these stars and are taken into account. Free-free opacity for He I, C I and II (Peach 1970) has been incorporated together with those for H and  $\text{H}^-$ , though only found to be important in the infrared and the deepest atmospheric regions with high temperatures.

Electron scattering and Rayleigh scattering (against H, He and C) are included in the source function  $S_\nu = (\kappa_\nu B_\nu + \sigma_\nu J_\nu) / (\kappa_\nu + \sigma_\nu)$ , with the first term representing the thermal emission and the second the scattering contribution.

### 2.2.2. Atomic and molecular line opacities

The effect of line-blanketing in these objects with their low hydrogen content and thus reduced continuous opacity may be expected to be important. Line data has been compiled from the millions of lines computed by Kurucz (1989) for the iron group elements (Ca-Ni) and tabulated for appropriate temperatures and damping pressures for giants and supergiants. Furthermore, absorption cross-sections from strong lines due to Na, Al, Mg and Si (Wiese et al. 1969) as well as carbon line data from the Opacity Project have been included, but found to be of minor importance compared to the other bound-bound transitions. All line opacities are treated with opacity sampling up to 450 nm, and beyond that the ODFs of Gustafsson et al. (1975) have been used. These ODFs were, however, calculated for a solar chemical composition. Due to the much higher mean molecular weight of the gas in these hydrogen-deficient stars, a solar composition ODF will *overestimate* the opacity in  $\text{m}^2 \text{kg}^{-1}$  for a given  $T - P_e$  point, which must be compensated for. Each ODF is multiplied with the molecular weight for the composition used in the calculation of the ODF at this  $T - P_e$ , and divided by the molecular weight for the (hydrogen-deficient) model atmosphere composition. The underabundance of hydrogen for the models compared to the ODFs causes an overestimate for this line opacity. However, the main share of the total line opacity is contributed by metals rather than hydrogen, and this effect is neglected.

Several molecules (CN, CO, C<sub>2</sub>, NH, MgH, CH, OH, SiH, SiO) have been considered, and their opacities are mainly included by means of ODFs. The amount of molecular opacity will probably be underestimated with the solar-like composition of the ODFs, since carbon and nitrogen are overabundant in these stars, while the hydrides do not contribute significantly to the molecular opacity for the relevant temperature range. Furthermore, for  $\lambda > 720 \text{ nm}$  only the line opacity from CO and CN have been computed (in  $\text{m}^2$  per molecule; hence those ODFs are not dependent on the chemical composition). Due to the relatively small contribution from molecules we believe that this omission will not have any significant effect on the resulting model atmospheres, except possibly for the coolest models.

## 3. Physical properties of the models

### 3.1. General characteristics

Some examples of typical model atmospheres are given in Fig. 1a–d. The temperature structures are steep indicating a large amount of backwarming. Many models therefore suffer from density and gas pressure inversions, which will be discussed in some detail in Sect. 3.2. Compared to models with the same parameters but with solar abundances the temperatures at depth are significantly higher (up to 2000 K) and due to the lower

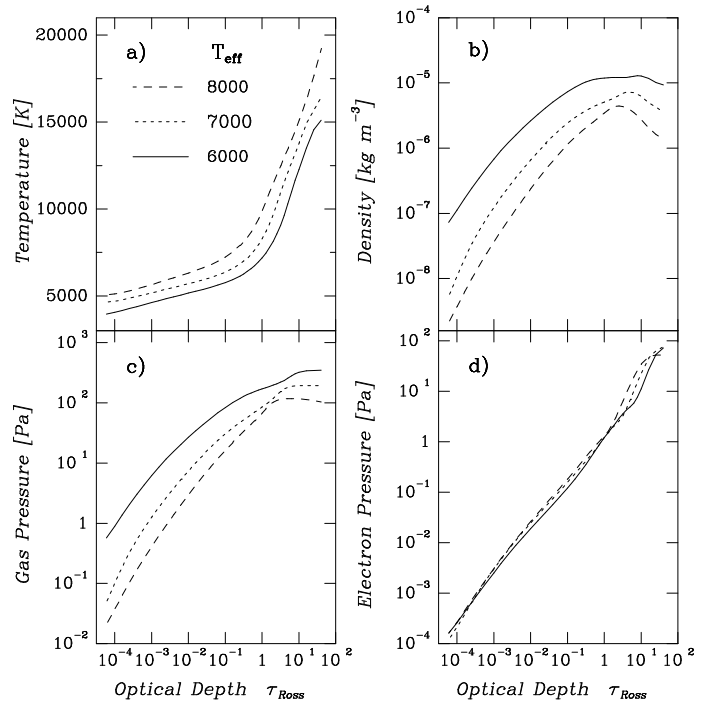


**Fig. 1a–d.** The atmospheric structures for three models with different  $T_{\text{eff}}$  showing: **a**  $T(\tau_{\text{Ross}})$ , **b**  $\rho(\tau_{\text{Ross}})$ , **c**  $P_{\text{gas}}(\tau_{\text{Ross}})$  and **d**  $P_e(\tau_{\text{Ross}})$ . All models have  $\log g = 0.5$  [cgs],  $\xi_{\text{turb}} = 5 \text{ km s}^{-1}$  and C/He=1%. Note the density and gas pressure inversions in the inner layers

continuous opacities the gas and electron pressures are much greater. Also evident from Fig. 1d is the independence of the electron pressure on the effective temperatures for  $\tau_{\text{Ross}} < 1$ , in spite of significant differences in the temperature and gas pressure structures. As  $T_{\text{eff}}$  increases, the temperature increases at all depths which leads to more ionization, but at the same time the continuous opacity becomes greater. Hence a smaller geometrical depth is encountered for a given  $\tau_{\text{Ross}}$  where the densities of electron donors are lower. These two opposite effects compensate each other for these models.

In Fig. 2 the most important opacity sources (Rosseland means for  $\tau_{\text{Ross}} > 0.5$  and Planck means for  $\tau_{\text{Ross}} < 0.5$ ) are plotted with C I bf controlling the absorption in the spectral line forming region while helium takes over in the inner layers. However, electron scattering dominates outside  $\tau_{\text{Ross}} \sim 0.05$  and causes the slow decrease in  $\kappa_{\text{Ross}}$  towards the surface. C<sup>-</sup> is not very important but He<sup>-</sup> can rival C I bf for models with a C/He ratio of 0.3% and lower or for low effective temperatures. Other significant elements are N and Mg. The ionization zone of carbon is seen in Fig. 2 as a decrease in opacity around  $\tau_{\text{Ross}} \sim 2$  before helium starts to contribute significantly in deeper layers. However, carbon ionization starts already at smaller optical depths, e.g.  $\sim 50\%$  of C is in the form of C II at  $\tau_{\text{Ross}} = 0.1$  for our reference model ( $T_{\text{eff}} = 7000 \text{ K}$ ,  $\log g = 0.5$  [cgs],  $\xi_{\text{turb}} = 5.0 \text{ km s}^{-1}$ , C/He=1%), but higher absorption coefficients for higher temperatures compensate the increased amount of ionization until carbon is almost completely ionized.

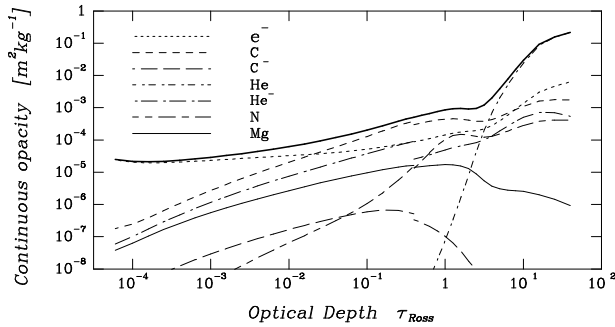


**Fig. 2.** The most important continuous opacity contributions as a function of depth for the reference model:  $T_{\text{eff}} = 7000$  K,  $\log g = 0.5$  [cgs],  $\xi_{\text{turb}} = 5$  km s $^{-1}$  and C/He=1%. The thick solid line represents the Rosseland mean opacity. The individual opacity sources are Rosseland weighted means for  $\tau_{\text{Ross}} > 0.5$  and Planck weighted means for  $\tau_{\text{Ross}} < 0.5$ . Notice the large discontinuity for He $^{-}$ , reflecting that the opacity is mainly located in the IR

Convection is a relatively inefficient energy transport mechanism at the low densities encountered in these atmospheres. For all models at most 1% of the total flux is carried by mixing length convection above  $\tau_{\text{Ross}} = 10$ , though the convective flux increases rapidly at greater depths in the He ionization zone. There is also convective motion present in the carbon ionization zone at  $\tau_{\text{Ross}} \sim 1$  but with negligible energy transport. Overshooting seems to be unimportant as seen by comparing the estimated cooling time scale ( $\tau_{\text{cool}} \approx (1 + (\rho\kappa H_{\text{P}})^2)/(16\sigma T^3 \kappa/c_{\text{p}})$ ) and the convective time scale ( $\tau_{\text{conv}} \approx H_{\text{P}}/v_{\text{conv}}$ ) for a rising element (e.g. Nordlund 1974), due to the low opacity  $\kappa$  and heat capacity  $c_{\text{p}}$  of the gas. Here we have assumed that the mixing length for a convection cell is roughly equal to the pressure scale height  $H_{\text{P}}$ . The uncertainty of the mixing length recipe should therefore probably be relatively unimportant, at least in the line-forming regions relevant for abundance analyses. Turbulent pressure due to large-scale convective motion and microturbulence is not included in the present models.

Typical values of the sound velocity in the models are about 5 km s $^{-1}$ , though slightly higher for  $\tau_{\text{Ross}} > 1$  and close to the surface ( $\tau_{\text{Ross}} < 10^{-3}$ ). This is unusually low for supergiants and is an effect of the high molecular weight. These low values may be compared to observed radial velocity variations for R CrB stars, with the largest amplitude found for RY Sgr with at least  $\Delta v_{\text{radial}} \approx \pm 20$  km s $^{-1}$  during a pulsation period, and the microturbulence parameters of typically 5-10 km s $^{-1}$  as found from abundance analyses. Both RY Sgr (Cottrell & Lambert 1982) and R CrB (Rao & Lambert 1996) show line doubling, which has been interpreted as a shock signature, which would be compatible with the calculated sound velocities here. Other R CrB stars with large velocity variations (with e.g.  $\Delta v_{\text{radial}} \approx \pm 15$  km s $^{-1}$  for V CrA and GU Sgr, Herbig 1994) should also show line doubling, at least for the strong lines, but this has not yet been reported.

### 3.2. Density inversions and super-Eddington luminosities

Due to the low densities and high luminosities experienced in the models, a density inversion occurs in the innermost layers ( $\tau_{\text{Ross}} \gtrsim 3$ ), as can be seen from Fig. 1b, which is related to the ionization zone of helium. It is also connected to the driving of the pulsations for these stars through the so called strange mode instabilities, where the pulsation energy is trapped inside the inversion zone (Gautschi & Glatzel 1990). A density inversion is not inhibited by a Rayleigh-Taylor instability, if convection is present (Glatzel & Kiriakidis 1993). Also, a gas pressure inversion reverses the direction of the local acceleration and therefore the criteria for a Rayleigh-Taylor instability are not fulfilled (Wentzel 1970).

Effects contributing to the occurrence of a density inversion (i.e.  $d\rho/dP_{\text{tot}} < 0$ ) can be found from a look at the equation of state, which we write as:

$$P_{\text{tot}} = P_{\text{gas}} + P_{\text{rad}} = \frac{\mathcal{R}\rho T}{\beta\mu} \quad (1)$$

to include the radiation pressure. Differentiating and rearranging leads to:

$$\frac{d \ln \rho}{d \ln P_{\text{tot}}} = \frac{d \ln \beta}{d \ln P_{\text{tot}}} + \frac{d \ln \mu}{d \ln P_{\text{tot}}} + (1 - \nabla), \quad (2)$$

where  $\nabla \equiv d \ln T / d \ln P_{\text{tot}}$  denotes the actual temperature gradient. The second term on the right hand side is always negative in an ionization zone. In our models the first term is negative and  $\nabla$  is greater than 1 in the upper layers of the density inversions which are seen in our models. The dominating term, however, is the one due to a changing molecular weight in our case. Although sometimes suggested in the literature (e.g. Maeder 1989), a density inversion is *not* caused by a local super-Eddington luminosity. Many stellar models show density inversion without a super-Eddington luminosity being present, though for some models these two phenomena may be present simultaneously. Both have their origin in an ionization zone, which causes a decrease in molecular weight (density inversion) and a high opacity (gas pressure inversion). For “normal” stars ionization of hydrogen and for R CrB stars ionization of He may cause such inversions in the atmospheres.

Proceeding towards lower gravities (higher luminosity-to-mass ratio) for a given effective temperature, one finds that the resulting model atmospheres first show a density inversion (at  $\log g = 3.5$  [cgs] for  $T_{\text{eff}} = 5000$  K and a R CrB star composition), followed by super-Eddington luminosities. The latter also result in gas pressure inversions, since hydrostatic equilibrium demands an inversion to occur to counterbalance the otherwise unstable situation. The Eddington limit is reached when the outwards directed radiative acceleration equals the gravitational acceleration inwards:  $\Gamma = g_{\text{rad}}/g = 1$  (our usage of the term the Eddington limit is defined by this condition. Originally, Eddington (1926) studied the case when electron scattering is the dominant opacity source, and therefore a more suitable term in the present case might be the opacity-modified Eddington limit). This does not, however, automatically cause

an outflow of material if  $\Gamma > 1$  occurs for  $\tau_{\text{Ross}} > 1$ , since a positive gas pressure gradient may compensate the negative radiation pressure gradient in hydrostatic equilibrium:

$$\frac{1}{\rho} \frac{dP_{\text{gas}}}{dr} = -g_{\text{eff}} = -g(1 - \Gamma), \quad (3)$$

with the radiative acceleration defined as

$$g_{\text{rad}} = \frac{1}{c} \int_0^{+\infty} \kappa_{\nu} \mathcal{F}_{\nu} d\nu, \quad (4)$$

$\mathcal{F}_{\nu}$  being the physical flux and  $\kappa_{\nu}$  the mass extinction coefficient (including scattering and with dimension  $\text{m}^2 \text{kg}^{-1}$ ). Crucial for a gas pressure inversion to develop is that the continuous opacity dominates the line opacity in the region, or else material is accelerated outwards as in the winds of hot stars. The realization that gas pressure inversions may develop is not new: an early discussion on the topic was given by Mihalas (1969). However, little progress has been reported regarding the stability of such an atmosphere.

At yet lower gravities the models are constrained by the requirement that the density and the gas pressure should not become negative. Numerical convergence problems for our models have prevented us from reaching this strict limit, and its location in the  $T_{\text{eff}}\text{--}\log g$  diagram can only be estimated by uncertain extrapolation. However, with our code there is no problem to construct model atmospheres with a super-Eddington luminosity locally. The opacity will not necessarily be dominated by electron scattering in the critical layers with  $g_{\text{eff}} < 0$ , as have sometimes been claimed in the literature (e.g. Humphreys & Davidson 1994; Nieuwenhuijzen & de Jager 1995), as our models demonstrate. Also, the density and gas pressure need not be zero, though the gas pressure *gradient* may be. Hence there is no direct reason why the Eddington limit cannot be achieved as a star evolves. However, it is possible that some kinds of instabilities occur as the star crosses the Eddington limit, or even somewhat earlier. Further work on the possibility of such instabilities is in progress and will be described elsewhere (Asplund, in preparation). Comparison with recently determined parameters of R CrB stars indeed suggests a connection between the Eddington limit and the decline events of the stars, and also a similarity between the R CrB stars and the Luminous Blue Variables, such as  $\eta$  Carinae and P Cygni (Asplund & Gustafsson 1996).

### 3.3. Effects of uncertainties in the fundamental parameters

Effective temperature estimates from observed line strengths in R CrB stars often have typical uncertainties of at least 250 K. In Fig. 3a the effect of such a change on the model structure is seen by comparing the models with  $T_{\text{eff}} = 6750$  and  $7250$  K with the reference model with  $T_{\text{eff}} = 7000$  K (all three for  $\log g = 0.5$ ). As expected, the higher the effective temperature the lower the gas pressure and density will be for a given optical depth, due to the increase in opacity for higher temperatures. At the surface the difference in temperature is only 300 K while at depth it

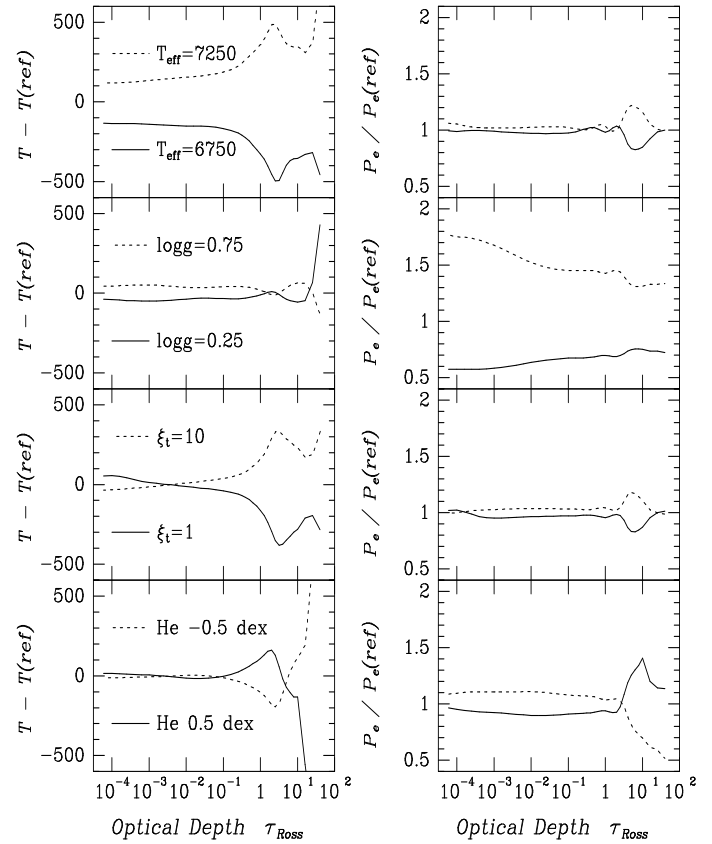


**Fig. 3a–d.** The effects on the model atmosphere when changing the fundamental parameters and abundances compared to the reference model with  $T_{\text{eff}} = 7000$  K,  $\log g = 0.5$  [cgs],  $\xi_{\text{turb}} = 5 \text{ km s}^{-1}$  and  $\text{C/He} = 1\%$ : **a** changes in  $T_{\text{eff}}$ , **b** in  $\log g$ , **c** in  $\xi_{\text{turb}}$  and **d** in  $\text{C/He}$  ratio. The left panels show the temperature variations compared to the reference model and the right panels the effects on the electron pressure

approaches 1000 K. The higher temperatures compensate the lower gas pressures for the warmer model by increasing the amount of ionization, which results in similar electron pressures, especially for  $\tau_{\text{Ross}} < 1$ .

In Fig. 3b the variations due to gravity changes are displayed. For the more extended models, the gas and electron pressures naturally become smaller as is immediately seen from the equation of hydrostatic equilibrium. The temperature structure remains roughly the same, though at depth the temperatures are slightly higher due to the less efficient convection for the low gravity models.

A change in the microturbulence parameter will affect the amount of backwarming, which is illustrated in Fig. 3c. The temperature and electron pressure in the outer layers are mainly unaltered but due to the greater blocking for larger line broadening the model with  $\xi_{\text{turb}} = 10 \text{ km s}^{-1}$  is about 500 K warmer in deep layers. Observed microturbulences for R CrB stars are  $\sim 5 - 10 \text{ km s}^{-1}$ , while our grid is calculated with  $5 \text{ km s}^{-1}$ , but the model difference will not be very large for the line-forming regions. Furthermore, if mass-loss is present, observed microturbulence parameters may be overestimated (Lamers & Achmad 1994).

### 3.4. Effects of abundance variations

A major problem in constructing model photospheres of R CrB stars is the large uncertainty in the C/He ratio due to the above-mentioned difficulty in determining the ratio from observations. In the outer layers, helium mainly acts as an inert element, since it only directly affects the gas pressure and molecular weight and does not influence the opacity or the number of free electrons. Therefore, a different He abundance is equivalent to a change in the surface gravity, as has previously been demonstrated for solar-type dwarfs by Strömgren et al. (1982). Following the discussion in Strömgren et al. (1982) we can derive a similar formula for hydrogen-deficient stars, if we assume the number densities of the elements to be  $N_C = N_N = 4N_O$  and ignore all other elements but He. If He is an inert element, provided the gravities of the two models with different C/He (number) ratios (here denoted by  $z$ ) are related by

$$g_2 = g_1 \cdot \frac{\left(1 + \frac{4}{30z_1}\right)}{\left(1 + \frac{4}{9z_1}\right)} \cdot \frac{\left(1 + \frac{4}{9z_2}\right)}{\left(1 + \frac{4}{30z_2}\right)}, \quad (5)$$

they should have similar  $T(\tau_{\text{Ross}})$  and  $P_e(\tau_{\text{Ross}})$  and hence show similar spectra. A change of C/He from 1% to 3% will have the same effect as an *increase* in  $\log g$  by 0.04, and therefore the same abundances would be derived when using these two models. Note that the changes are opposite compared to the corresponding case with solar abundances, since increasing C/He also increases  $P_e$  for a given  $\tau_{\text{Ross}}$  due to more ionization of carbon. The computed models are indeed similar in their  $P_e(\tau_{\text{Ross}})$  structures, but some temperature variations arise since  $P_{\text{gas}}(\tau_{\text{Ross}})$  is very different in the two models. With a higher C/He,  $P_{\text{gas}}(\tau_{\text{Ross}})$  is lower and hence pressure broadening is relatively less important. Therefore the amount of backwarming decreases which causes the temperature difference of about 200 K at  $\tau_{\text{Ross}} = 1$ . This also explains the difference in flux distribution and photometric colours between models with different C/He ratios, as described below in Sect. 5 and Sect. 6.

Since  $\kappa_{\text{Ross}}$  will be higher when increasing the C/He ratio, lower densities and gas pressures will result. Counterbalancing the smaller densities, an increased amount of ionization of carbon leaves the electron pressure less affected than the gas pressure. A higher C/He ratio diminishes the importance of the line opacity and less backwarming is to be expected, which is supported by Fig. 3d. However, at great depths this decreased backwarming is offset by the less efficient convection, due to the lower densities, which increases the temperature.

With the hydrogen abundance adopted for the standard models ( $\log \epsilon_{\text{H}} = 7.50$ ) this element is a trace element and no change is apparent when decreasing it further. However, a significantly higher hydrogen content, as in e.g. V854 Cen, will affect the models since the importance of the opacity contributed by H rivals the bound-free absorption from both He I and C I. The increased opacity will lower the densities and gas pressures for  $\tau_{\text{Ross}} > 1$  the same way as a higher C/He ratio does. A H-abundance of 11.00 decreases the densities and pressures for  $\tau_{\text{Ross}} < 1$  by some 20-40%. The diminished importance of

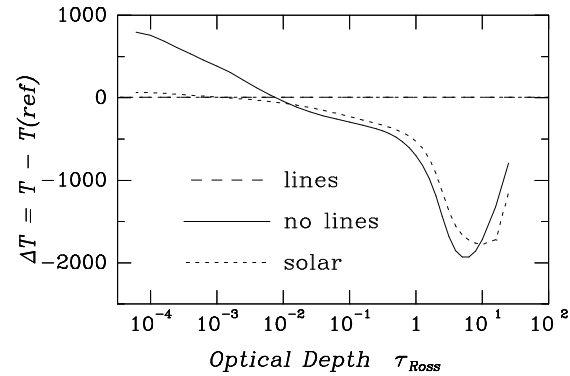


**Fig. 4.** The temperature difference when neglecting all line opacity (solid) compared to our reference model with  $T_{\text{eff}} = 7000$  K,  $\log g = 0.5$  [cgs],  $\xi_{\text{turb}} = 5$  km s $^{-1}$  and C/He=1% (dashed). Also shown is the effect when using solar abundances instead (dotted)

the line opacity leads to significantly lower temperatures for  $\tau_{\text{Ross}} > 0.01$ , while closer to the surface the smaller amount of surface cooling due to lines shows up. At  $\tau_{\text{Ross}} = 1$  the temperature difference is 500 K but further in it can reach 1 500 K, compared with our reference model. In Fig. 4 the temperature difference between a model with solar abundances and one with an R CrB composition is plotted, vividly showing the steep temperature gradient for the hydrogen-deficient stars.

### 3.5. Effects of line blanketing

The effects of line-blanketing on the model atmospheres of R CrB stars are severe and strongly limits the usefulness of non-blanketed models. With a deficiency of hydrogen, the continuous opacity is reduced relative to the line opacity, which leads to a relatively larger importance of lines. The difference relative to a model without the line opacity is illustrated in Fig. 4, which shows a backwarming of 2 000 K and a surface cooling of 750 K for our reference model. This should be compared with the effect on a model with the same stellar parameters but with solar abundances rather than a typical R CrB composition. In this case the backwarming and surface cooling amounts to 900 K and 800 K respectively.

An uncertainty in the present models is of course the use of ODFs with solar-like metallicity for wavelengths between 450 nm and 720 nm (beyond 720 nm only ODFs containing CO and CN opacities are used which are tabulated per molecule). However, the typical composition of a R CrB star is roughly similar to the solar case (Lambert & Rao 1994), with the obvious exception of hydrogen, which does not contribute the main fraction of the line opacity. Therefore, a drastically different total line opacity for R CrB-like ODFs compared to the ones used here is not expected when using the above-mentioned compensation for the difference in molecular weight.

Only some 200 carbon lines are included in the present study with the OS technique and only for  $\lambda < 450$  nm with data taken from the Opacity Project. Ignoring this line-opacity has no effect on the computed models ( $\Delta T < 1$  K). It is possible that a veil

of many more weak carbon lines in the visual and infrared could modify the model structures but we find it less likely that they cause a major effect in view of the small effects of the carbon lines taken into consideration. Carbon is a relatively simple atom and strong effects from a wealth of weak lines not included here are not expected.

### 3.6. Effects of sphericity

Due to the large luminosity-to-mass ratio encountered in these stars, the atmospheres are extended and the effect of sphericity may be significant. Following Gustafsson et al. (1975) a zero order estimate of the temperature effects is obtained from the differences in flux and radius:

$$0 = \frac{\Delta \mathcal{F}}{\mathcal{F}} \approx \frac{4\Delta T}{T_{\text{eff}}} + \frac{2\Delta R}{R_*}. \quad (6)$$

For our reference model with  $T_{\text{eff}} = 7000$  K and  $\log g = 0.5$ , the temperature corrections would be  $-140$  K,  $-90$  K,  $-60$  K and  $-30$  K at  $\log \tau_{\text{Ross}} = -4, -3, -2$ , and  $-1$ , respectively, assuming  $M_* = 0.85 M_{\odot}$ . Naturally, the more extreme models at lower  $\log g$  will have larger relative temperature changes. In Fig. 5a we present the relative thickness of the atmosphere  $\Delta z/R_*$  (with the thickness defined as  $\Delta z = R(\tau_{\text{Ross}} = 10^{-4}) - R(\tau_{\text{Ross}} = 10)$ ) for different parameters, assuming a stellar mass of  $0.85 M_{\odot}$  (as suggested by evolutionary and pulsational studies of R CrB stars, such as Weiss 1987a,b). A simple rule of thumb is that the sphericity effects become significant for  $\Delta z/R_* \geq 10\%$ . The figure suggests that the plane-parallel approximation can be justified for  $\log g \geq 0.0$  [cgs] and  $T_{\text{eff}} \leq 7000$ . For higher  $T_{\text{eff}}$ 's significant sphericity effects set in at somewhat higher gravities.

For comparison we have included relevant continuous opacities in the spherical model atmosphere code *SOSMARCS* and in the plane-parallel version *PLAMARCS* of B. Plez (both entirely OS and also based on the original *MARCS*-code of Gustafsson et al. 1975, Plez et al. 1992), though without the important line-blanketing. The agreement between *PLAMARCS* and our code when neglecting the line opacity is very good. The spherical models (assuming  $M_* = 0.85 M_{\odot}$ ) are, as expected, cooler at the surface compared to the corresponding plane-parallel models and have roughly the same temperature structure at depth (less than 100 K warmer), which is seen in Fig. 5b. The temperature corrections are only slightly larger than those estimated following Eq. 6, while the gas pressure is actually about 10% larger at a given optical depth. This is due to the lower  $\kappa_{\text{Ross}}$  resulting from the lower temperatures, but the electron pressures are lower by about the same amount due to less ionization. The flux distributions of the two models show no significant difference. It is expected that the inclusion of atomic and molecular lines would make the atmosphere more extended and cool the surface even further. New spherical, hydrogen-deficient opacity sampling model atmospheres are under construction.

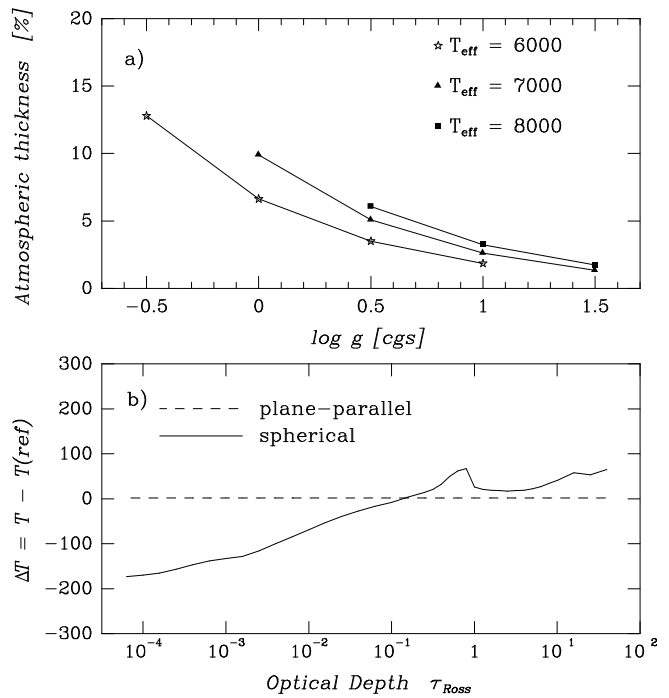


**Fig. 5.** **a** The thickness of the model atmosphere as defined by  $[R(\tau_{\text{Ross}} = 10^{-4}) - R(\tau_{\text{Ross}} = 10)]/R_*$  for different temperatures and gravities. The stellar mass is assumed to be  $0.85 M_{\odot}$ . **b** The temperature differences when using spherical symmetry (solid) rather than plane-parallel (dashed) model atmosphere codes for our reference model. Only continuous opacities are included and  $M_* = 0.85 M_{\odot}$  has been assumed

### 3.7. Effects of departures from LTE

The present models are based on the LTE assumption and its relevance must be questioned in these supergiants. The most important element is carbon and Asplund & Ryde (1996) have therefore investigated possible departures from LTE for this element with a restricted NLTE analysis (i.e. statistical equilibrium calculations with LTE model atmospheres) using *MULTI* (Carlsson 1986) and a very extensive model atom with 217 atomic levels and 453 radiative transitions. The effects are found to be small, especially in the line-forming region (Asplund & Ryde 1996), in fact smaller than for the Sun. The NLTE population for any atomic level of carbon differs by less than 10% compared to the LTE value in the line forming region ( $\log \tau_{\text{Ross}} \geq -2.5$ ), and not at all for the lowermost levels of C I and C II. The derived carbon abundances from optical absorption lines have typical NLTE correction factors smaller than 0.05 dex. The basic reason for the small departures from LTE is the low  $J_{\nu}/B_{\nu}$  values in the UV region as a result of the severe line-blocking, which prevent strong photoionization. Significant overionization of carbon which would have affected the structure of the models is therefore probably not present. Also, the much higher densities in R CrB stars than in stars with normal solar-like abundances with similar fundamental parameters increase the importance of collisions and hence tend to restore LTE. Therefore, the assump-

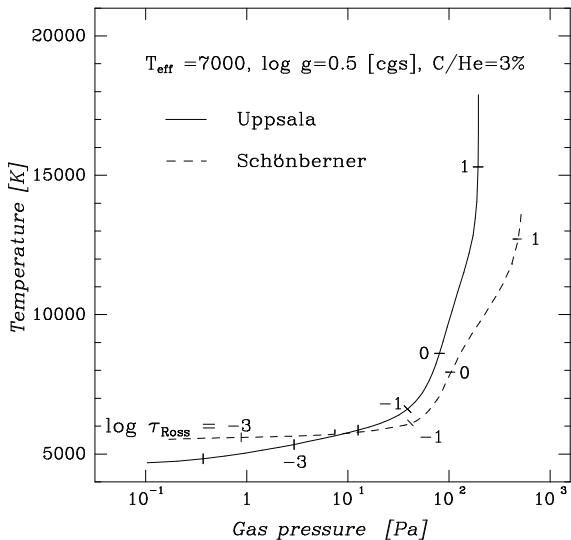


**Fig. 6.** Comparison of a line-blanketed model atmosphere (solid) with a Schönberner model (dashed) with the same parameters ( $T_{\text{eff}} = 7000$ ,  $\log g = 0.5$  [cgs] and  $C/\text{He}=3\%$ ). Rosseland optical depths are marked along the curves

tion of LTE seems to be a fair approximation, perhaps somewhat surprisingly considering the low gravities.

#### 4. Comparison with previous models

A reasonable treatment of the line-blanketing in model atmospheres of R CrB stars has long been urged. The models of Schönberner (1975) contain no line-blanketing. Jones (1991) modified an existing MARCS-code (Gustafsson et al. 1975) to include more continuum opacity sources but the lines were only treated through solar-metallicity ODFs and with now outdated continuum opacities. Furthermore, Jones seems not to have compensated the hydrogen-rich ODFs for the very different molecular weight in R CrB stars as described above. Neither Schönberner nor Jones have published their models and only used them for abundance analysis. The effort to track down Jones' models proved unsuccessful and hence we can only comment on the differences between our models and Schönberner's.

Due to the neglect of line opacity, Schönberner's models are much more compact and lack the steep temperature gradient of the present models. These differences can be seen in Fig. 6 for a model with  $T_{\text{eff}} = 7000$  K and  $\log g = 1.0$  [cgs] and with the same chemical composition ( $C/\text{He}=3\%$ ). At the surface ( $\log \tau_{\text{Ross}} = -3.6$  in Schönberner's model) the temperature is 400 K cooler in the present model while at the bottom of the atmosphere the increased backwarming results in a temperature difference larger than  $\sim 2000$  K. This enables our models to reproduce observed features such as  $\text{C}_2$  and He lines with consistent parameters, in contrast to non-blanketed models. The higher continuous opacities in our models result in lower gas pressures, except for close to the surface where the higher temperatures in the non-blanketed model leads to a higher  $\kappa_{\text{Ross}}$ . The electron pressures are larger in our models

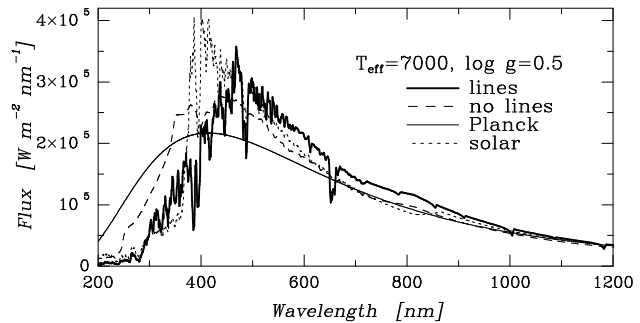


**Fig. 7.** The flux distribution of our reference model (thick solid) compared to a blackbody distribution with the same temperature (thin solid), an R CrB model with only continuum opacities (dashed) and a line-blanketed model with solar abundances (dotted)

in the line-forming regions due to the higher temperatures and hence larger ionization. Schönberner's models are very similar to models computed with our program if the line opacity is neglected.

#### 5. Comparison of calculated and observed flux distribution

The large amount of line opacity forces parts of the flux in the UV towards longer wavelengths, which is illustrated in Fig. 7. For clarity all model atmosphere fluxes are smoothed with a rectangular passband with  $\Delta\lambda = 2$  nm and the fluxes in the ODFs have been randomly distributed within each ODF before smoothing to avoid unrealistic bias with wavelength. Compared to the Planck distribution for the same temperature and the flux from the model with only continuum opacity, the flux distribution of our reference model looks very different. As a result too low  $T_{\text{eff}}$ 's are estimated for R CrB stars from photometry when only using Planck curves or non-blanketed model fluxes (e.g. Goldsmith et al. 1990). Compared to normal stars, R CrB stars suffer significantly more line-blocking as seen in Fig. 7, which explains their redder colours. The flux distributions of R CrB models are less sensitive to the adopted gravity but the models with a smaller  $C/\text{He}$  ratio are bluer as a result of being hotter in the continuum forming layer due to increased backwarming.

It is important to compare the model fluxes with observed fluxes, in order to estimate whether the model atmospheres describe the stars adequately. For this purpose spectrophotometric data for the eponymous star R CrB close to pulsational maximum were kindly provided by N.K. Rao. The flux measurements were dereddened using  $E(B-V)=0.05$  (Rao 1995) and Seaton's interstellar reddening curve (Seaton 1979). Ultraviolet fluxes have been obtained from the *IUE* Uniform Low Dispersion Archive, and we have used the good quality observation of August 17, 1979, with the LWR camera ( $\Delta\lambda = 0.6$  nm), when R CrB was out of minimum and at a similar pulsational phase as at the time of the visual observations. The data was dereddened the same way as the visual fluxes. The J and H magnitudes were taken from the literature (Glass 1978), which causes some uncertainty since the visual and IR fluxes are not necessarily measured at the same pulsational phase. However, the light am-

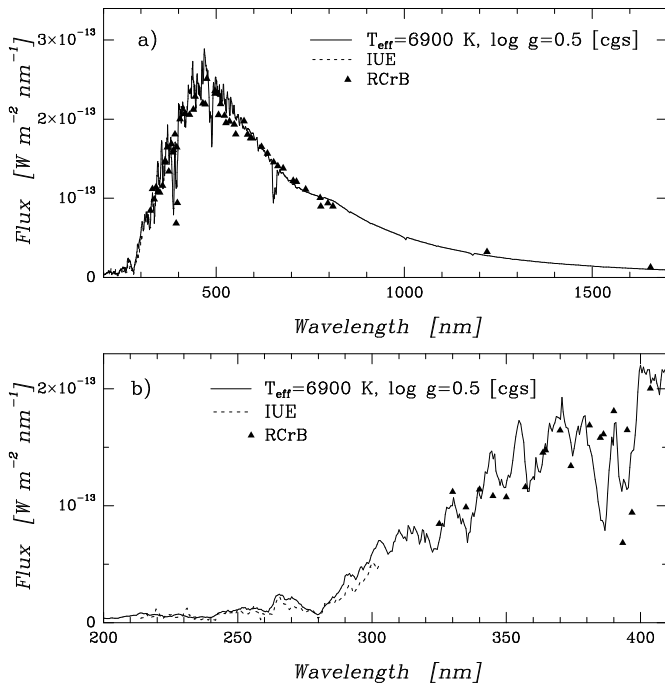


**Fig. 8.** **a** Comparing the narrow-band fluxes (triangles) of R CrB with our best fit with  $T_{\text{eff}} = 6900$  K and  $\log g = 0.5$  [cgs] (solid line). Infrared magnitudes were taken from Glass (1978), while ultraviolet fluxes (dashed) were obtained from the *IUE* Ultraviolet Low Dispersion Archive. **b** An enlargement of the ultraviolet region

plitude is small for R CrB,  $\Delta V \simeq 0.2$ , and should be even less for the J and H bands.

In Fig. 8 the observed fluxes of R CrB are compared to the best fitted model with  $T_{\text{eff}} = 6900$  K and  $\log g = 0.5$  [cgs], and using the individual abundances for the star (Lambert et al, in preparation) rather than the abundances in Table 1, but still assuming  $C/He=1\%$ . The overall agreement is clearly very satisfactory, even in the UV region, and certainly shows a much more realistic flux distribution than the non-blanketed models previously published (e.g. Goldsmith et al. 1990). The fit cannot carefully constrain the gravity of the star, though the situation improves slightly if one instead uses  $C/He=0.3\%$  and  $T_{\text{eff}} = 6800$  K. The latter is due to shifting part of the flux towards shorter wavelengths since the backwarming increases with a lower  $C/He$  ratio (see above). The quality of the fits using different  $C/He$  ratios does not, however, admit any estimate of the  $C/He$  ratio for R CrB with the present observations. One can imagine though that carefully comparing the flux distributions together with spectroscopic analysis of various  $T_{\text{eff}}$  and  $\log g$  indicators could allow an estimate of the  $C/He$  ratio.

Even for the best fit to R CrB the model overestimates the fluxes slightly around  $\lambda = 500$  nm. One should remember however, that synthetic spectra have not been used longwards of 450 nm and, for example, the  $C_2$  absorption in this wavelength region may be too small when using ODFs. In the infrared there seems to be too little model flux. This discrepancy corresponds to about 16% of the total flux at J ( $0^m 16$ ) and 21% at H ( $0^m 21$ ).

It could either be due to circumstellar material or different observing epochs for the visual fluxes and the IR magnitudes. The errors in the IR flux calibration could also be partly responsible. The larger disagreement at longer wavelengths suggests the influence of circumstellar dust.

If the excess is due to circumstellar material one may estimate its blackbody temperature to  $T_{\text{bb}} \approx 2000$  K, which is not far from the dust condensation temperature and higher than the characteristic temperature for the circumstellar shell which typically is 700 K (Kilkenny & Whittet 1984). Hence we may be witnessing the effect of recent dust formation off the line-of-sight before it has been accelerated outwards and cooled down. If we assume the dust to be optically thin for IR wavelengths we can estimate the mass of the dust cloud from the formula

$$M_{\text{dust}} = \frac{4d^2 \mathcal{F}_\lambda}{\kappa_\lambda B_\lambda(T_{\text{dust}})}, \quad (7)$$

which is derived from the Kirchhoff-Planck law. Here  $d$  is the distance (assuming  $M_V = -5$ ),  $\mathcal{F}_\lambda$  the excess flux and  $\kappa_\lambda$  the dust opacity (in  $\text{m}^2 \text{kg}^{-1}$ ) adopted from Koike et al (1980) for amorphous carbon, which is the type of dust believed to form around R CrB stars (e.g. Hecht et al 1984). The estimated  $M_{\text{dust}}$  is then  $\sim 10^{-11} M_\odot$ , which corresponds to  $\sim 10^{-8} M_\odot$  for the mass of the cloud if 10% of all C condenses into dust, which is in agreement with previous estimates (e.g. Feast 1986).

There are a few other discrepancies between the observed and calculated model fluxes, most notably around  $H\alpha$  and  $H\beta$  where the ODFs naturally largely overestimate the opacity. Around the Ca II H and K lines there also seems to be too little model flux, which is probably due to a combination of a large amount of atomic lines in the region and a large Ca-resonance from the Opacity Project data (the latter is seen in the fluxes for a model with only continuous opacities). Interestingly, the spectral region corresponds roughly to the unidentified extended emission found for RY Sgr during two different deep minima (Alexander et al. 1972; Asplund 1995).

From the observed photometry and the infrared flux method, we can estimate an effective temperature of R CrB of 6600 K. For this exercise we have used model atmospheres with the individual abundances of R CrB rather than the standard abundances of the grid models. If there is a contribution from dust emission in the infrared the effective temperature will be higher. Assuming all the excess light in J and H compared to the model fluxes being due to circumstellar dust, we derive a temperature of 6900 K. We emphasize, however, the uncertainty which arises when all fluxes are not obtained at the same epoch.

## 6. Photometry

No theoretical photometry for hydrogen-deficient stars has previously been published, which has prevented easy estimates of effective temperatures for a large sample of these stars. We publish here such data, however, only based on model fluxes instead of detailed synthetic spectra as a first step. Our primary calibration source is a Vega-model ( $T_{\text{eff}} = 9650$ ,  $\log g = 3.90$  [cgs],  $[Fe/H] = 0.0$ ,  $\xi_{\text{turb}} = 2.0 \text{ km s}^{-1}$ , Dreiling & Bell 1980) which

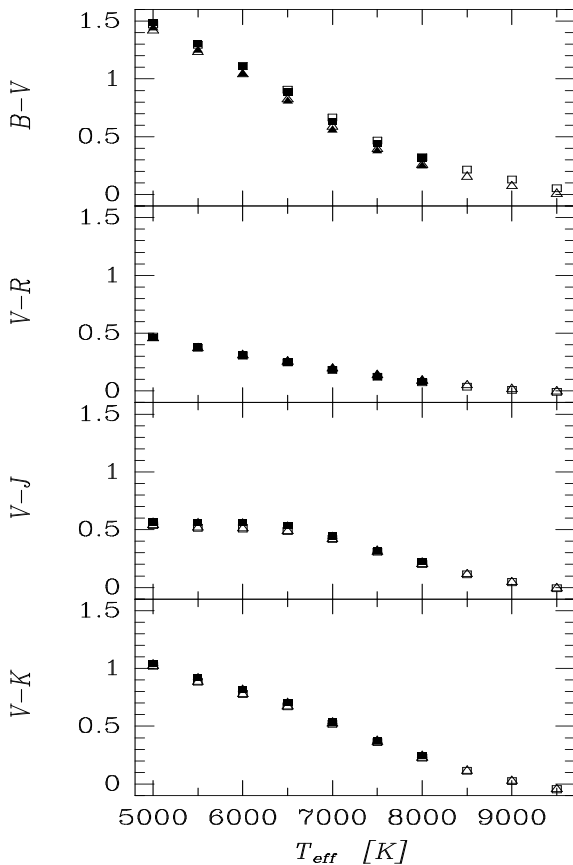


**Fig. 9.** The  $B - V$ ,  $V - R$ ,  $V - J$  and  $V - K$  colours as functions of  $T_{\text{eff}}$  for selected models with different  $\log g$  and  $C/\text{He}$  ratios. Squares refer to  $C/\text{He}=1\%$  while triangles represent  $C/\text{He}=0.3\%$ . Open symbols are for  $\log g = 1.0$  [cgs] and filled symbols  $\log g = 0.5$  [cgs]

we define to have all colours equal to 0.00. As a test of the accuracy of the derived photometric data we have compared a solar model ( $T_{\text{eff}} = 5780$ ,  $\log g = 4.44$  [cgs],  $[\text{Fe}/\text{H}] = 0.0$ ,  $\xi_{\text{turb}} = 1.0 \text{ km s}^{-1}$ ) with observations and found gratifying agreement, e.g.  $(B - V)_{\text{model}} = 0.67$  and  $(B - V)_{\text{obs}} = 0.63 - 0.69$  (Hayes 1985), also for the IR colours. The transmission filters used for the computations were those of Bessell (1990) for  $UBVRI$  and Bessell & Brett (1988) for  $JHKLM$ . Before the calculations of the colours, the fluxes within each ODF (10 nm wide) have been randomized to avoid unphysical bias with wavelength; all models have the same randomization with wavelength. In Fig. 9 we present  $B - V$ ,  $V - R$ ,  $V - J$  and  $V - K$  as a function of effective temperature for different gravities and  $C/\text{He}$  ratios.

The  $B - V$  colour is a good measure of the effective temperature. However, it is also dependent on  $C/\text{He}$  and gravity. A lower  $C/\text{He}$  ratio increases the backwarming, see Fig. 3d, which decreases  $B - V$  for a given  $T_{\text{eff}}$ . On the other hand, decreasing  $\log g$  cools the surface slightly, which explains the higher  $B - V$ . The importance of the line blanketing in these hydrogen-deficient stars is seen by comparing with the colours for models with solar abundances which have about 0.4 lower  $B - V$  for the same stellar parameters.

$V - R$  is rather insensitive to gravity changes and its behaviour with  $T_{\text{eff}}$  is similar to  $B - V$ . However, the dependence of  $V - R$  on  $C/\text{He}$  is opposite that of  $B - V$ : a smaller ratio leads to slightly higher  $V - R$ . This may, however, well be an effect of the use of ODFs in the colour calculations.  $V - J$  and  $V - K$  are not very dependent on  $C/\text{He}$ , but are rather sensitive to gravity changes, in particular for the low effective temperatures. This is an effect of the increased amount of absorption from CO and CN in the IR, due to the higher densities for higher  $\log g$ . In fact, the  $V - J$  curve flattens out as  $T_{\text{eff}}$  goes below about 6000 K when molecular absorption becomes very significant. Due to the use of ODFs, the colours may be systematically affected and the values presented here should be taken as preliminary.

### 6.1. Comparison between observed and theoretical colours

We now compare the observed colours of R CrB stars and HdC stars with observed colours in order to estimate effective temperatures. Some uncertainty arises when comparing with spectroscopically derived values due to different pulsational phases, which can change  $T_{\text{eff}}$  significantly. Furthermore, abundance variations between those used for the grid presented here and the individual stellar abundances may cause systematic errors in the determination of the stellar parameters.

During a pulsational period of R CrB,  $(B - V)_0$  varies between 0.46 and 0.56 (Ferne & Seager 1994; Rao 1995). From Fig. 9 we estimate  $T_{\text{eff}}$  to vary between 7200 and 7400 K, assuming  $C/\text{He}=1\%$ . For a lower  $C/\text{He}$  of 0.3% these values would be about 200 K lower. Reasonable changes of the gravity leads to revisions of  $T_{\text{eff}}$  by less than 100 K. These photometrically estimated  $T_{\text{eff}}$ 's are significantly greater than those derived from IRFM (6600-6900 K, see discussion above), flux fitting (6900 K) and spectroscopic analysis (6250-6750 K, Rao & Lambert 1996). However, it should be remembered that the colours in Fig. 9 are calculated from the models with the standard abundances given in Table 1. Using the  $B - V$  colours from model atmospheres with the individual abundances of R CrB (Lambert et al, in preparation),  $T_{\text{eff}}$  varies between 6800 and 7100 K during a period, which is in better agreement with the other methods. The difference in photometric colours for R CrB are due to lower abundances of metals in R CrB compared to the standard abundances used for the grid models, which decreases the line-blocking in the UV and blue. Again assuming  $C/\text{He}=0.3\%$  instead of 1% would further lower the temperatures by about 100 K. The temperature difference that still remains between the photometry and the other temperature indicators may be due to an underestimate of, for example, the  $\text{C}_2$  opacity in the models, which would make the  $B - V$  colours systematically too high for  $T_{\text{eff}} \lesssim 7000$  K. Fig. 8 supports this since the observed fluxes are smaller than the model predictions around 500 nm.

In Table 3 we present  $B - V$  colours and reddening estimates (Lawson et al 1990; Rao 1995) for some R CrB and HdC stars, together with the estimated effective temperatures as judged from  $B - V$ . V854 Cen and HD 148839 are not included due to their unusual high H abundances compared to other members

**Table 3.** Photometry and estimated effective temperatures of some RCB and HdC stars

Star	$(B - V)$	$E(B - V)$	$T_{\text{eff}}(B - V)$ [K]	$T_{\text{eff}}^a$ [K]
V3795 Sgr <sup>b</sup>	0.98	0.79	8 500	8 000
VZ Sgr <sup>b</sup>	0.73	0.50	8 300	7 800
UW Cen	0.65	0.32	7 900	7 400
RY Sgr	0.47	0.13	7 900	7 400
UV Cas	1.37	1.01	7 800	7 300
Y Mus	0.92	0.50	7 700	7 200
UX Ant	0.55	0.06	7 400	6 900
XX Cam	0.87	0.27	7 100	6 600
SU Tau	1.10	0.50	7 100	6 600
V CrA <sup>b</sup>	0.73	0.14	7 100	6 600
RS Tel	0.81	0.17	7 000	6 500
RZ Nor	1.16	0.51	7 000	6 500
RT Nor	1.11	0.39	6 800	6 300
GU Sgr	1.19	0.37	6 700	6 200
U Aqr	0.95	0.05	6 500	6 000
S Aps	1.21	0.05	5 900	5 400
WX CrA	1.26	0.06	5 800	5 300
HD 173409	0.89	0.05	6 600	6 100
HD 182040	1.05	0.05	6 100	5 600
HD 175893	1.15	0.05	6 000	5 500
HD 137613	1.19	0.05	5 900	5 400

<sup>a</sup> The photometrically estimated  $T_{\text{eff}}$ 's have been subtracted by 500 K to agree better with the spectroscopically obtained values (Lambert et al., in preparation), see text

<sup>b</sup> Star has different chemical composition compared to the majority of RCB stars (Lambert & Rao 1994)

of the class, which make their  $B - V$  colours bluer for a given  $T_{\text{eff}}$ . Some uncertainty in  $T_{\text{eff}}$  arises due to the  $B - V$  dependence on gravity and C/He ratio, as well as the poorly known reddening, both interstellar and circumstellar. When comparing these values with estimates from a recent abundance analysis of warm R CrB stars (Lambert et al., in preparation), one finds that the photometric colours systematically give larger  $T_{\text{eff}}$ 's by about 500 K. Therefore, all temperatures in the fifth column in Table 3 have been subtracted by 500 K to better agree with the spectroscopic values. We attribute the difference to a too high metallicity for the present models, which increases the blocking in the blue and UV and hence makes the colours redder. Typically, the abundances derived using these model atmospheres are 0.5 dex smaller (Lambert et al., in preparation) compared to for non-blanketed models (Lambert & Rao 1994) on which the abundances used here have been based. As seen above for R CrB, using the individual abundances for each star makes the spectroscopically and photometrically determined parameters agree within the expected errors. This is further seen by noting the larger discrepancy for the different  $T_{\text{eff}}$ 's for VZ Sgr and V CrA with the temperature estimates differing by about 1 000 K. Both have significantly lower Fe abundances compared to the majority of R CrB stars (Lambert & Rao 1994), which decreases  $B - V$  further. Unfortunately, no reliable temperatures have

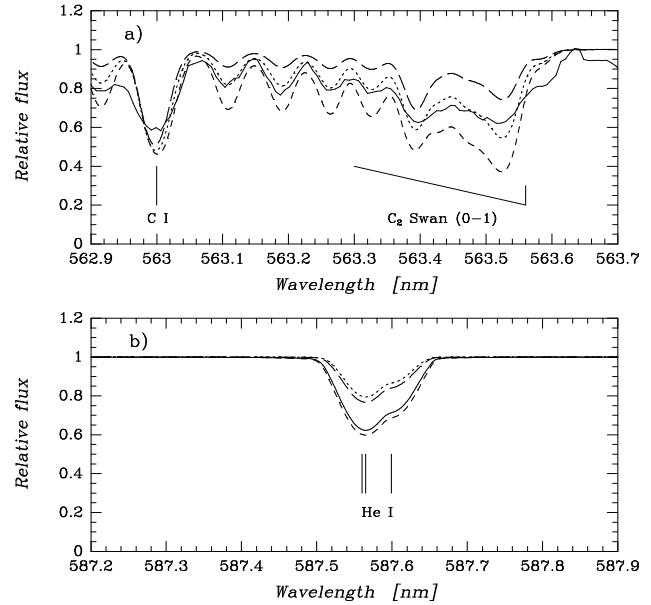


**Fig. 10.** **a** The observed  $C_2$  Swan (0-1) band around 563.5 nm in the R CrB star V482 Cyg (solid) compared to synthetic spectra of three models:  $T_{\text{eff}} = 6 500$ ,  $\log g = 0.5$  [cgs] (dotted);  $T_{\text{eff}} = 6 500$ ,  $\log g = 1.0$  [cgs] (short dashed);  $T_{\text{eff}} = 7 000$ ,  $\log g = 1.5$  [cgs] (long dashed). All models have C/He=1.0%. Notice the insensitivity on stellar parameters of the strength of the C I line at 563.0 nm. **b** The helium triplet at 587.6 nm for four different models with  $T_{\text{eff}} = 7 000$ ,  $\log g = 1.0$  [cgs] (dotted);  $T_{\text{eff}} = 7 000$ ,  $\log g = 0.5$  [cgs] (long dashed);  $T_{\text{eff}} = 8 000$ ,  $\log g = 1.0$  [cgs] (solid); and  $T_{\text{eff}} = 8 000$ ,  $\log g = 0.5$  [cgs] (dashed)

been published for the HdC stars, which prevents a discussion on the consistency between photometry and spectroscopy for those stars.

Finally, we once again emphasize that synthetic spectroscopy has not been employed here for the calculation of the colours, which could possibly introduce systematic effects. Therefore care must be exercised when using the photometry presented and the colours should be considered as preliminary. There is, for example, an obvious problem with the theoretical  $V - J$  and  $V - K$  since the observed colours are significantly larger, which is also seen in colour-colour diagrams. This could indicate an underestimate of the assumed reddening, contamination by circumstellar material or possibly that detailed synthetic spectroscopy is necessary. Further work to resolve this question is in progress.

## 7. Synthetic spectroscopy

The steep temperature gradient of R CrB stars is perhaps best illustrated by the emergent spectra. Observed R CrB stars show the presence of  $C_2$  even for as high effective temperatures as 7 000 K, and for the same temperature He I and C II lines are visible. The computed synthetic spectra show strong molecular bands, due to e.g.  $C_2$  in agreement with observations. In Fig. 10a synthetic spectroscopy of the  $C_2$  Swan (0-1) band at 563.5 nm

are presented for three different models and compared with observations for the R CrB star V482 Cyg. The synthetic spectra have been convolved with a gaussian profile with a width of  $10 \text{ km s}^{-1}$ , representing both the instrumental profile and the macroturbulence in the star, and only line opacity due to C<sub>2</sub> and C I has been included. The strength of the band head can be well fitted with either a model with  $T_{\text{eff}} = 6500 \text{ K}$  and  $\log g = 0.5$  [cgs] or  $T_{\text{eff}} = 6750 \text{ K}$  and  $\log g = 1.3$  [cgs]. In the same figure one can also notice the insensitivity of the strengths of the C I lines on the stellar parameters as a result of the continuous opacity being due to atomic levels of carbon with similar excitation energies as the observed lines. However, the observed line in Fig. 10a is significantly weaker than the predicted values using the input carbon abundance, as for all other C I lines. This problem is further discussed in Gustafsson & Asplund (1996) and in Lambert et al. (in preparation).

In the IR, CO vibration-rotation bands are predicted to be visible up to  $T_{\text{eff}} \approx 7000 \text{ K}$ , though they may be masked by the emission from the circumstellar dust shell, in particular for the fundamental bands around  $4.3 \mu\text{m}$ . The first overtone of CO around  $2.3 \mu\text{m}$  should be present for cooler  $T_{\text{eff}}$  than about  $6500 \text{ K}$ , which is also seen for several of the cooler R CrB and HdC stars (Asplund et al., in preparation). Sphericity is likely to further cool the surface and hence make such molecular bands visible in spectra of slightly hotter models.

The high temperatures encountered at depth enables both lines due to helium and singly ionized carbon to be present. In Fig. 10b the helium triplet blend at  $587.5 \text{ nm}$  is plotted for four models with  $T_{\text{eff}} = 7000$  and  $8000 \text{ K}$  and  $\log g = 0.5$  and  $1.0$  [cgs]. In reality the helium feature is blended by neighbouring C I lines but this has been ignored in the figure. The Boltzmann factor for the He I line will be a factor 10 larger (the temperature difference is about  $500 \text{ K}$  in the line-forming region) in line-blanketed R CrB models compared to both non-blanketed models and models with solar abundances as seen in Fig. 4, and hence makes the line visible even at low effective temperatures.

## 8. Concluding remarks

We have presented new line-blanketed model atmospheres for hydrogen-deficient stars, such as R CrB and HdC stars, to be used for abundance analysis and for investigation of the atmospheric stability. The line opacity and improved continuous opacities greatly affect the models and make the temperature gradients much steeper than for previously published models. This explains the presence of molecular bands (e.g. C<sub>2</sub>) even for effective temperatures as high as  $7000 \text{ K}$ , and at the same time the observed lines of helium and ionized carbon in R CrB stars.

We have compared the flux distributions for our models with narrow-band photometry in the visual and IUE spectra in the ultraviolet for R CrB and found a good agreement with a model with  $T_{\text{eff}} = 6900 \text{ K}$ . In the infrared the observed magnitudes are greater than what the models predict, which we interpret as either being due to additional circumstellar material between the stellar surface and the circumstellar shell or possibly different pulsational phase for the different observations. The former

explanation could correspond to recently formed dust close to the stellar photosphere with a temperature around  $2000 \text{ K}$  and a dust mass of  $\sim 10^{-11} M_{\odot}$ . Therefore, our measurement of the effective temperature for R CrB through the infrared flux method is rather uncertain: a temperature of  $6600 \text{ K}$  is obtained if all the excess light originates in the star, while  $6900 \text{ K}$  is obtained if the excess is assumed to be caused by circumstellar gas. Effective temperatures estimated from the photometry presented here are systematically higher by about  $500 \text{ K}$  compared to values obtained from spectroscopy. The difference is mainly due to a too large metallicity by about  $0.5 \text{ dex}$  being used for the model atmospheres, but possibly also due to the neglect of detailed synthetic spectroscopy.

The large luminosity-to-mass ratio for the R CrB stars makes the models sensitive to the radiative acceleration. All computed models show a density inversion caused by the ionization of helium, but some low gravity models also experience a gas pressure inversion as an effect of the outwards directed radiative acceleration locally exceeds the gravity. This interesting phenomenon could be a trigger mechanism to the famous decline events of R CrB stars where gas close to the stellar surface condenses to dust and obscures the star. Further investigations and comparisons with observed parameters of R CrB stars are in progress (Asplund & Gustafsson 1996; Asplund, in preparation).

Even though the models represent a significant improvement as compared with previously existing models, it should be remembered that these models still are very rough approximations to the real stellar atmospheres. Progress in relaxing a few of the assumptions and approximations made here is currently being made, in particular spherical symmetry is included in the models and the atomic and molecular line opacity is improved, which should increase the realism of the models further. Eventually, however, the inclusion of hydrodynamics coupled to radiative transfer may be necessary to properly model these pulsating supergiants.

*Acknowledgements.* The authors appreciate a fruitful collaboration with D.L. Lambert and N.K. Rao with both stimulating discussions and kind sharing of observational data. The project was initiated when BG was the Beatrice Tinsley guest professor at the University of Texas, Austin, and the support from its Department of Astronomy is gratefully acknowledged. B. Edvardsson, S. Jeffery, B. Plez, K. Pollard and N. Ryde are thanked for their help during the project. MA thanks P. Woitke for inspiring discussions on the R CrB phenomena. The importance of opacity data from the Opacity Project and R.L. Kurucz is acknowledged, as well as the opacity data received prior to publication from T.L. John.

## References

- Alexander J.B., Andrews P.J., Catchpole R.M., Feast M.W., Lloyd Evans T., Menzies J.W., Wisse P.N.J., Wisse M., 1972, MNRAS 158, 308
- Asplund M., 1995, A&A, 294, 763
- Asplund M., Gustafsson B., 1996, in: Hydrogen-deficient stars, Jeffery C.S., Heber U. (eds.). ASP conf. series vol. 96, p. 39

- Asplund M., Ryde N., 1996, in: Hydrogen-deficient stars, Jeffery C.S., Heber U. (eds.). ASP conf. series vol. 96, p. 57
- Bell K.L., Hibbert A., Berrington K.A., 1988, *JPhysB*, 21, 2319
- Bessell M.S., 1990, *PASP*, 102, 1181
- Bessell M.S., Brett J.M., 1988, *PASP*, 100, 1134
- Carlsson M., 1986, Uppsala Astronomical Observatory Report No. 33
- Cottrell P.C., Lambert D.L., 1982, *ApJ*, 432, 785
- Cunto W., Mendoza C., Ochsenein F., Zeppen C.J., 1993, *A&A*, 275, L5
- Dreiling L.A., Bell R.A., 1980, *ApJ*, 241, 736
- Eddington A.S., 1926, *The internal constitution of the stars*, Cambridge University Press, p. 115
- Edvardsson B., Andersen J., Gustafsson B., Lambert D.L., Nissen P.E., Tomkin J., 1993, *A&A*, 275, 101
- Feast M.W., 1986, in: Hydrogen-deficient stars and related objects, Hunger K., Schönberner D., Rao N.K. (eds.). Reidel, Dordrecht, p. 151
- Fernie J.D., Seager S., 1994, *PASP*, 106, 1138
- Gautschy A., Glatzel W., 1990, *MNRAS*, 245, 597
- Glatzel W., Kiriakidis M., 1993, *MNRAS*, 263, 375
- Glass I.S., 1978, *MNRAS*, 185, 23
- Goldsmith M.J., Evans A., Albinson J.S., Bode M.F., 1990, *MNRAS*, 245, 119
- Gustafsson B., Asplund M., 1996, in: Hydrogen-deficient stars, Jeffery C.S., Heber U. (eds.). ASP conf. series vol. 96, p. 27
- Gustafsson B., Bell R.A., Eriksson K., Nordlund Å., 1975, *A&A*, 42, 407
- Hayes D.S., 1985, in: Calibration of fundamental stellar quantities, Hayes D.S., Pasinetti L.E., Philip A.G.D. (eds.). Reidel, Dordrecht, IAU Symp. 111, p. 225
- Heber U., 1986, in: Hydrogen-deficient stars and related objects, Hunger K., Schönberner D., Rao N.K. (eds.). Reidel, Dordrecht, p. 33
- Hecht J.H., Holm A.V., Donn B., Wu C.C., 1984, *ApJ*, 280, 228
- Herbig G., 1994, private communication
- Humphreys R.M., Davidson K., 1994, *PASP*, 106, 1025
- Jeffery C.S., Heber U., 1993, *A&A*, 270, 167
- Jeffery C.S., Heber U., Hill P.W., Pollacco D., 1988, *MNRAS*, 231, 175
- John T.L., 1975, *MNRAS*, 172, 305
- John T.L., 1994, *MNRAS*, 269, 871
- Jones K., 1991, PhD thesis, St Andrews University
- Kilkenny D., 1982, *MNRAS*, 200, 1019
- Kilkenny D., Whittet D.C.B., 1984, *MNRAS*, 208, 25
- Koike C., Hasegawa H., Manabe A., 1980, *Ap&SS*, 67, 495
- Kurucz, R.L., 1989, private communication
- Lambert D.L., Rao N.K., 1994, *JA&A*, 15, 47
- Lamers H.J.G.L.M., Achmad L., 1994, *A&A*, 291, 856
- Lawson W.A., Cottrell P.L., Kilmartin P.M., Gilmore A.C., 1990, *MNRAS*, 247, 91
- Leuenhagen U., Hamann W.-R., 1994, *A&A*, 283, 567
- Lombard F., Koen C., 1993, *MNRAS*, 263, 309
- Loreta E., 1934, *Astron. Nachr.*, 254, 151
- Maeder A., 1989, in: Physics of luminous blue variables, Davidson K., Moffat A.F.J., Lamers H.J.G.L.M. (eds.). Kluwer, Dordrecht, p. 15
- Mihalas D., 1969, *ApJ*, 156, L155
- Nieuwenhuijzen H., de Jager C., 1995, *A&A*, 302, 811
- Nordlund Å., 1974, *A&A*, 32, 407
- Peach G., 1970, *MemRAS*, 73, 1
- Plez B., Brett J.M., Nordlund Å., 1992, *A&A*, 256, 551
- Ramsbottom C.A., Bell K.L., Berrington K.A., 1992, *JPhysB*, 25, 1443
- Rao N.K., 1995, private communication
- Rao N.K., Lambert D.L., 1996, preprint
- Renzini A., 1979, in: Stars and star systems, Westerlund B.E. (ed.). Reidel, Dordrecht, p. 155
- Schönberner D., 1975, *A&A*, 44, 383
- Seaton M.J., 1979, *MNRAS*, 187, 73P
- Seaton M.J., Yan Y., Mihalas D., Pradhan A.K., 1994, *MNRAS*, 266, 805
- Strömgren B., Olsen E.H., Gustafsson, B., 1982, *PASP*, 94, 5
- Warner B., 1967, *MNRAS*, 137, 119
- Webbink R.F., 1984, *ApJ*, 277, 355
- Weiss A., 1987, *A&A*, 185, 165
- Weiss A., 1987, *A&A*, 185, 178
- Wentzel D.G., 1970, *ApJ*, 160, 373
- Whitney B.A., Clayton G., Schulte-Ladbeck R.E., Meade M.R., 1992, *AJ*, 103, 1652
- Wiese W.L., Smith M.W., Miles B.M., 1969, Atomic Transition Probabilities, NSRDS-NBS 22